polysaccharides

MDPI

Review

Post-Combustion Capture of Carbon Dioxide by Natural and Synthetic Organic Polymers

Sudip Kumar Ghosh * and Moumita Ghosh *

Department of Chemistry, Techno India University, Kolkata 700091, India
* Correspondence: sudip.k@technoindiaeducation.com (S.K.G.); moumita.g@technoindiaeducation.com (M.G.)

Abstract: The elevation of carbon dioxide (CO_2) levels in the atmosphere is responsible for global warming which in turn causes abrupt climate change and consequently poses a threat to living organisms in the coming years. To reduce CO_2 content in the atmosphere CO_2 capture and separation is highly necessary. Among various methods of CO_2 capture post-combustion capture is very much useful because of its operational simplicity and applicability in many industries and power sectors, such as coal-fired power plants. Polymers with high surface area, high volume and narrow pores are ideal solid sorbents for adsorption-driven post-combustion CO_2 capture. Natural polymers, such as polysaccharides are cheap, abundant, and can be modified by various methods to produce porous materials and thus can be effectively utilized for CO_2 capture while the surface area and the pore size of synthetic porous organic polymers can be tuned precisely for high CO_2 capturing capacity. A significant amount of research activities has already been established in this field, especially in the last ten years and are still in progress. In this review, we have introduced the latest developments to the readers about synthetic techniques, post-synthetic modifications and CO_2 capture capacities of various biopolymer-based materials and synthetic porous organic polymers (POPs) published in the last five years (2018–2022). This review will be beneficial to the researchers to design smart polymer-based materials to overcome the existing challenges in carbon capture and storage/sequestration.

Keywords: carbon dioxide capture; post-combustion; polysaccharide; synthetic polymer

check for updates

Citation: Ghosh, S.K.; Ghosh, M. Post-Combustion Capture of Carbon Dioxide by Natural and Synthetic Organic Polymers. *Polysaccharides* **2023**, *4*, 156–175. https://doi.org/10.3390/polysaccharides4020012

Academic Editor: Karin Stana Kleinschek

Received: 25 January 2023
Revised: 23 March 2023
Accepted: 16 May 2023
Published: 31 May 2023

Copyright: © 2023 by the authors. Licensee MDPI, Basel, Switzerland. This article is an open access article distributed under the terms and conditions of the Creative Commons Attribution (CC BY) license (https://creativecommons.org/licenses/by/4.0/).

1. Introduction

A major threat to the inhabitants of the earth is global warming which is primarily responsible for climate change. Global warming is mainly caused by increasing concentrations of carbon dioxide (CO_2) gas in the atmosphere with time. CO_2 emissions rose to a historic high in recent years mostly due to the burning of fossil fuels [1]. To prevent the increase in the concentration of CO_2 in the atmosphere, carbon capture and storage/sequestration (CCS) is highly necessary. In general, the strategies used to capture CO_2 are pre-combustion, post-combustion, oxy-fuel combustion and direct air capture. Out of these strategies, post-combustion capture of CO_2 is operationally simple and useful in many industries and power sectors, such as coal-fired power plants [2]. Adsorption of gas onto the surface of solid material is considered an effective method for post-combustion CO_2 capture. Among various types of solid sorbents polymer and polymer-based materials are found to be highly promising. The use of non-toxic, cheap and widely available biopolymers such as cellulose, lignin, cyclodextrin, chitosan etc to capture CO_2 is an effective and highly sustainable carbon capture strategy while low density, high porosity, large surface area and high stability of synthetic organic polymers make them a good choice of materials for post-combustion carbon dioxide capture as well [3]. Surface modification of the POPs can also be performed easily to enhance CO_2 capture capacities. Porous biopolymer-based materials are usually prepared by carbonization and physical or chemical activation of the chosen biopolymer such as cellulose, chitosan, lignin, cyclodextrin, etc. Synthetic organic

polymers are generally obtained by connecting monomers by covalent bonds utilizing various types of reactions. The pore size and the nature of the surface can be tuned precisely by the selection of monomers and synthetic procedures to enhance CO_2 adsorption capacity and selectivity of CO_2 over other gases [3].

As CCS is an important and frontier area of research, a huge number of articles have been published in the last two decades. Development of new types of POPs and novel porous materials derived from them is going on rapidly worldwide. Some good review articles have been reported in the last decade on the syntheses and applications of POPs on CCS [3–6]. In this scenario, a comprehensive report is required to introduce to the readers the latest developments on the synthesis of various types of POPs and new materials derived from bio and synthetic polymers and their applications towards CCS. For this purpose, we have summarized synthetic techniques, post-synthetic modifications and CO_2 capture capacities of various biopolymer-based materials and synthetic POPs published in the last five years (2018–2022). Furthermore, we briefly mentioned the factors which influence CO_2 capture capacity and selectivity.

2. Mechanism of Adsorption and Related Thermodynamic Factors

There are two processes of adsorption, namely physical adsorption or physisorption and chemical adsorption or chemisorption. Physisorption occurs on the surface of the adsorbent via non-covalent interactions (Coulombic, Van der Waals, etc.) between adsorbate molecules and the surface. Desorption of the gas molecules in this case is a low-energy consumption process. The major advantage of physisorption is adsorbents can be reused easily while the disadvantages include less selectivity and low adsorption capacity of the adsorbent at high temperatures. In chemisorptions, covalent bonds are formed between gas molecules and the surface of the adsorbent. Common adsorbents contain basic functional groups such as amine on the surface of the material. Basic functional groups react with acidic CO_2 molecules producing salts. The major advantage of chemisorption is high adsorption capacity and good selectivity of the adsorbents. A common drawback of this process is the regeneration of sorbents consumes a lot of energy [7].

Isosteric heat of adsorption (Q_{st}) is indicative of the strength of interaction between adsorbents and CO_2 molecules. Q_{st} is calculated by fitting adsorption isotherms by using the Clausius–Clapeyron equation. A low Q_{st} value suggests predominant physisorption, whereas, a high Q_{st} value indicates a strong interaction between gas molecules and the material's surface leading to predominant chemisorption. Good adsorbents should selectively adsorb CO_2 over all other gases to achieve effective separation. Thus CO_2/N_2 selectivity is an important index for CO_2 capture by adsorbents. In practical applications, CO_2/N_2 selectivity is calculated by the initial slope method (Henry's law) and ideal adsorption solution theory (IAST). Flue gas released from power stations consists of 10–15% CO_2 and a large quantity of N_2. Therefore, effective CO_2-capturing materials should have a high affinity for CO_2 at low pressure and high CO_2/N_2 selectivity. The porosity and surface area of the adsorbents are also important factors which affect adsorption performance. The surface areas of the adsorbents are typically analyzed using Brunauer–Emmett–Teller (BET) theory [8].

3. Polysaccharide-Based Biopolymers for CO_2 Capture

Biopolymers are crowned with biocompatibility and biodegradability which can be utilized for designing biomaterials for various applications such as packaging materials in the food industry, fuel cells, drug delivery, membrane and medical implants organ preperation, tissue engineering and many more [9–14]. Polysaccharides are carbohydrate-based biopolymers which act as the most important source of energy in animal and plant biosystems. Among multiple applications of polysaccharides [15–19], one of the most important is CO_2 capture. Considering from an environmental and economic perspective polysaccharides are cheap and abundant [3,20–22] which perfectly outfits sustainable development

goals (SDGs) by the implementation of bio-based materials for environment cleaning and healthy living.

3.1. Cellulose

Cellulose is a linear polysaccharide consisting of repeated D-glucose units with the formula of $(C_6H_{10}O_5)_n$. In a recent study, bottom-up ecosystem simulation is coupled with models of cellulosic biofuel production, carbon capture and storage to track ecosystem and supply chain carbon flows for current and future biofuel systems. This approach could have climate mitigation and stabilization potential [20]. Qaroush et al. have discussed in detail different types of polysaccharides for CO_2 capture describing the reversible reaction between cellulose and CO_2, their subsequent dissolution, regeneration and CO_2 capturing using functionalised cellulosic materials [3]. One interesting approach is converting cellulose to sustainable porous carbon materials which is further applied for CO_2 capture [21]. Porous carbonaceous materials are usually prepared by carbonization and activation [21]. The carbonization process again can be of two types, namely (i) conventional pyrolytic approach which is heating the sample at elevated temperatures of 400–1000 °C in an inert atmosphere (e.g., N_2, Ar). This involves dehydration, condensation and isomerization, which eliminates most of the hydrogen and oxygen atoms to form H_2O, H_2, CH_4, and CO gases. (ii) Hydrothermal carbonization (HTC) is the other approach which is usually performed at moderate temperatures (<300 °C) and is advantageous due to reduced energy consumption, sample does not need to be dry and gives carbon-rich hydrochars in high yields. Thus in recent times, the HTC method is considered an energy-saving and environmentally friendly approach for carbonization [21]. Two activation methods are being reported which produce porous carbons with large differences in porosity. In general, physical activation processes create porous carbons with moderate surface areas (1000 m^2/g) and narrow micropores that can be beneficial for, e.g., CO_2/N_2 and CO_2/CH_4 separation [21]. In contrast, chemical activation significantly increases the surface area (up to >3000 m^2/g) and pore volume of the porous carbons which can be useful for gas storage [21]. Here we discuss the CO_2 adsorption capacity of some cellulose-derived materials derived by the carbonization process. In this regard, Heo et al. reported a series of porous carbons derived from commercial cellulose fibres in three steps and described that steam molecules played a key role in the pore-opening process and induced an increase in the surface area of the porous carbon materials formed. The cellulose fibres were carbonized under N_2 atmosphere followed by physical activation with steam under gauge pressure. Ultramicropores (pore size < 0.8 nm) were resulted by physical activation process which significantly contributed to the increase in surface areas from 452 to 540 m^2/g for pre-activated samples to 599–1018 m^2/g for steam-activated samples causing CO_2-over-N_2 adsorption selectivity and increase in CO_2 adsorption capacity [22]. This study was followed by Zhuo et al. who reportedly prepared hierarchically porous carbons by carbonization/activation of cellulose aerogels under CO_2 and N_2 atmosphere with improved surface area and volume for CO_2 adsorption and further showed that steam activation is an efficient process to prepare cellulose-based porous carbons with high CO_2 adsorption capacities [23].

Chemically activated carbonaceous materials have grabbed attention because of much higher surface areas resulting in much higher CO_2 adsorption capacities. Sevilla et al. reported on the chemical activation of cellulose by KOH thus designing microporous carbon materials with a very high surface area of 2370 m^2/g and CO_2 adsorption capacity of 5.8 mmol g^{-1} at 1 bar and 273 K at a high adsorption rate and excellent adsorption recyclability. They designed the material by hydrothermal carbonization of potato starch, cellulose and eucalyptus sawdust followed by chemical activation using potassium hydroxide [24]. Xu et al. have applied algae-extracted nanofibrous chemically modified cellulose carbonized under N_2 and CO_2 atmosphere and activated in CO_2 with significantly higher surface areas (832–1241 m^2/g) and higher volumes of ultramicropores (0.24–0.29 cm^3/g) for CO_2 adsorption [25]. Recent years have seen a promising application of cellulose aerogels in carbon storage. Ho et al. have reported a review [26] depicting a chemical

modification of nanocellulose aerogels that led to a large surface area which improved selectivity towards CO_2 adsorption. Kamran et al. have developed highly porous carbons by hydrothermal carbonization method and chemical activation using acetic acid as an additive. The cellulose-based materials showed high specific surface area (SSA) (1260–3019 $m^2\ g^{-1}$), microporosity in the range of 0.21–1.13 $cm^3\ g^{-1}$ with CO_2 adsorption uptake of 6.75 mmol g^{-1} and 3.96 mmol g^{-1} at 273 K and 298 K at 1 bar, respectively, and CO_2 selectivity. They reported that micropores between 0.68 nm and 1 nm exhibit high CO_2 adsorption potential [27].

However non-carbonized cellulose-derived materials have also been reported for efficient CO_2 adsorption capacities. In this regard, cross-linking of nanocellulose enhances the surface area and CO_2 adsorption was observed by Wang et al. and Sun et al. [28,29]. Amino-functionalized nanocellulose aerogels although had a reduced surface area still displayed chemisorption of CO_2 with a capacity of more than 2 mmol g^{-1} [26]. In some other reports, cellulose hybrids were designed without any carbonization with inorganic fillers such as silica, zeolite and metal–organic frameworks which improved the surface area and physisorption of CO_2 [26]. Sepahvand et al. have reported nano filters by a combination of cellulose nanofibers (CNF) and chitosan (CS) at varied loading compositions. They reported that increasing the concentration of modified CNFs increases the adsorption rate of CO_2 and the highest adsorption of CO_2 belonged to the 2% modified CNF [30]. A most recent study by Chen et al. reports epoxy-functionalized polyethyleneimine modified epichlorohydrin-cross-linked cellulose aerogel having a rich porous structure with a specific surface area in the range of 97.5–149.5 m^2/g. This material showed good adsorption performance, with a maximum CO_2 adsorption capacity of 6.45 mmol g^{-1} [31]. Material type and composition, BET surface area ($m^2\ g^{-1}$), pore size (nm)/total pore volume ($cm^3\ g^{-1}$), mechanism of adsorption, CO_2 capture capacity (mmol g^{-1}) and special features of cellulose-based materials have been tabulated in Table 1.

Table 1. Summary of material type and composition, BET surface area ($m^2\ g^{-1}$), pore size (nm)/total pore volume ($cm^3\ g^{-1}$), mechanism of adsorption, CO_2 capture capacity (mmol g^{-1}) and special features of cellulose-based materials.

Material Type and Composition	BET Surface Area ($m^2\ g^{-1}$)	Pore Size (nm)/Total Pore Volume ($cm^3\ g^{-1}$)	Mechanism of Adsorption	CO_2 Capture Capacity (mmol g^{-1})	Special Features	Ref
Porous carbons derived from commercial cellulose fibres	540 and 1018	<0.8 nm–/0.234 and 0.429	for pre-activated samples for steam-activated samples	3.776 at 298 K	CO_2-over-N_2 adsorption selectivity	[22]
Carbonized and activated cellulose from cotton linter	1364	1.42	physisorption	3.42	-	[23]
Chemically activated cellulose	2200–2400	1.1	physisorption	4.8	CO_2-over-N_2 adsorption selectivity	[24]
Algae extracted nanofibrous chemically modified cellulose activated in CO_2	832–1241	0.24–0.29	physisorption	2.29 at 0.15 bar, 5.52 at 1 bar; 273 K	CO_2-over-N_2 adsorption selectivity	[25]
Silica/Cellulose Nanofibril aerogel functionalized with 3-aminopropyl triethoxysilane	11	0.05	Chemisorption via reaction between amine group and CO_2	2.2 at humid condition	high chemisorption of CO_2 with reduced surface area	[26]

Table 1. *Cont.*

Material Type and Composition	BET Surface Area (m^2 g^{-1})	Pore Size (nm)/Total Pore Volume (cm^3 g^{-1})	Mechanism of Adsorption	CO_2 Capture Capacity (mmol g^{-1})	Special Features	Ref
Highly porous cellulose by hydrothermal method and chemical activation using acetic acid as an additive.	1260–3019	0.21–1.13	physisorption	6.75 at 273 K, 1 bar and 3.96 at 298 K, 1 bar	CO_2 selectivity	[27]
polyethyleneimine-crosslinked cellulose (PCC) aerogel sorbent	234.2	-	Surface diffusion and intra-particle diffusion mechanism	2.31 at 25 °C under pure dry CO_2 atm	Adsorption-desorption recyclability	[28]
Cellulose nanofiber (CNF) surface was functionalized using chitosan (CS), poly [β-(1, 4)-2amino-2-deoxy-Dglucose]	~360	~4 nm	Physisorption	4.8	Increasing the concentration of modified CNFs increases the adsorption rate of CO_2	[30]
Epoxy-functionalized polyethyleneimine modified epichlorohydrin-cross-linked cellulose aerogel	97.5–149.5	-	Chemisorption	6.45	Material showed preferable rigidity and carrying capacity	[31]

One important class of nanocellulose-based materials and their subsequent application involves membrane separation of CO_2. Ansaloni et al. reported micro fibrillated cellulose/Lupamin membrane which showed very good CO_2 permeability but the selectivity CO_2/N_2 and CO_2/CH_4 (in the order of 500 and 350, respectively, for pure micro cellulose) was compromised thus decreasing the overall membrane performance [32]. Venturi et al. later investigated the influence of doping in nanocellulose-based materials and performed a systematic study of CO_2 permeability by the newly designed membranes. They blended the commercial Polyvinylamine solution Lupamin® 9095 (BASF) with Nano Fibrillated Cellulose (NFC) which resulted in films. They observed that increasing water vapour and a higher presence of Lupamin in the film resulted in an improvement of both CO_2 gas permeability and selectivity. NFC content of 70 wt% Lupamin showed a selectivity of 135 for the separation of CO_2/CH_4 and 218 for CO_2/N_2. The maximum permeability in the order of 187 Barrer was reached at 80% RH [33]. In a later study, the addition of l-arginine to a matrix of carboxymethylated nano-fibrillated cellulose (CMC-NFC) resulted in a mobile carrier facilitated transport membrane for CO_2 separation. They reported that l-arginine (45 wt% loading) greatly improved CO_2 permeability by 7-fold from 29 to 225 Barrer and selectivity with respect to N_2 from 55 to 187 compared to pure carboxymethyl nanocellulose matrix [34] [Figure 1]. Hussain et al. have worked with pure and mixed matrix membranes (MMMs) to capture carbon from natural gas. They used polyethylene glycol (PEG), Multi-walled carbon nanotubes (MWCNTs) and cellulose acetate (CA) to prepare membranes of pure CA, CA/PEG blend of different PEG concentrations (5%, 10%, 15%) and CA/PEG/MWCNTs blend of 10% PEG with different MWCNTs concentrations (5%, 10%, 15%). They observed that CO_2/CH_4 selectivity is enhanced 8 times for pure membranes containing 10% PEG and 14 times for MMMs containing 10% MWCNTs and in mixed gas experiments, the CO_2/CH_4 selectivity is increased 13 times for 10% PEG and 18 times for MMMs with 10% MWCNT [35]. Mubashir et al. have developed composite membranes using non-stoichiometric ZIF-62 MOF glass and cellulose acetate (CA) which exhibited pore size (7.3 Å) and significant CO_2 adsorption on the unsaturated metal nodes [36]. In more recent studies, Rehman et al. have reported the synthesis of mixed matrix membranes (MMMs) by incorporating (1–5 wt%) Cu-MOF-GO composites as filler into cellulose acetate (CA) polymer matrix by adopting the solution casting method. They reported 1.79 mmol g^{-1} and 7.98 wt% of CO_2 uptake at 15 bar [37]. Some other foam-like cellulose composites have also been reported to capture CO_2. Wang et al. designed a strong foam-like composite by

the in situ growth of thermally stable and microporous metal–organic frameworks (MOFs) including copper benzene-1,3,5-tricarboxylate [$Cu_3(BTC)_2$], zinc 2-methylimidazolate, and aluminium benzene-1,3,5-tricarboxylate in a mesoporous cellulose template derived from balsa wood. The TO-wood/$Cu_3(BTC)_2$ composite shows high durability during the temperature swing cyclic CO_2 adsorption/desorption process and a high CO_2 adsorption capacity of 1.46 mmol g^{-1} at 25 °C and atmospheric pressure [38].

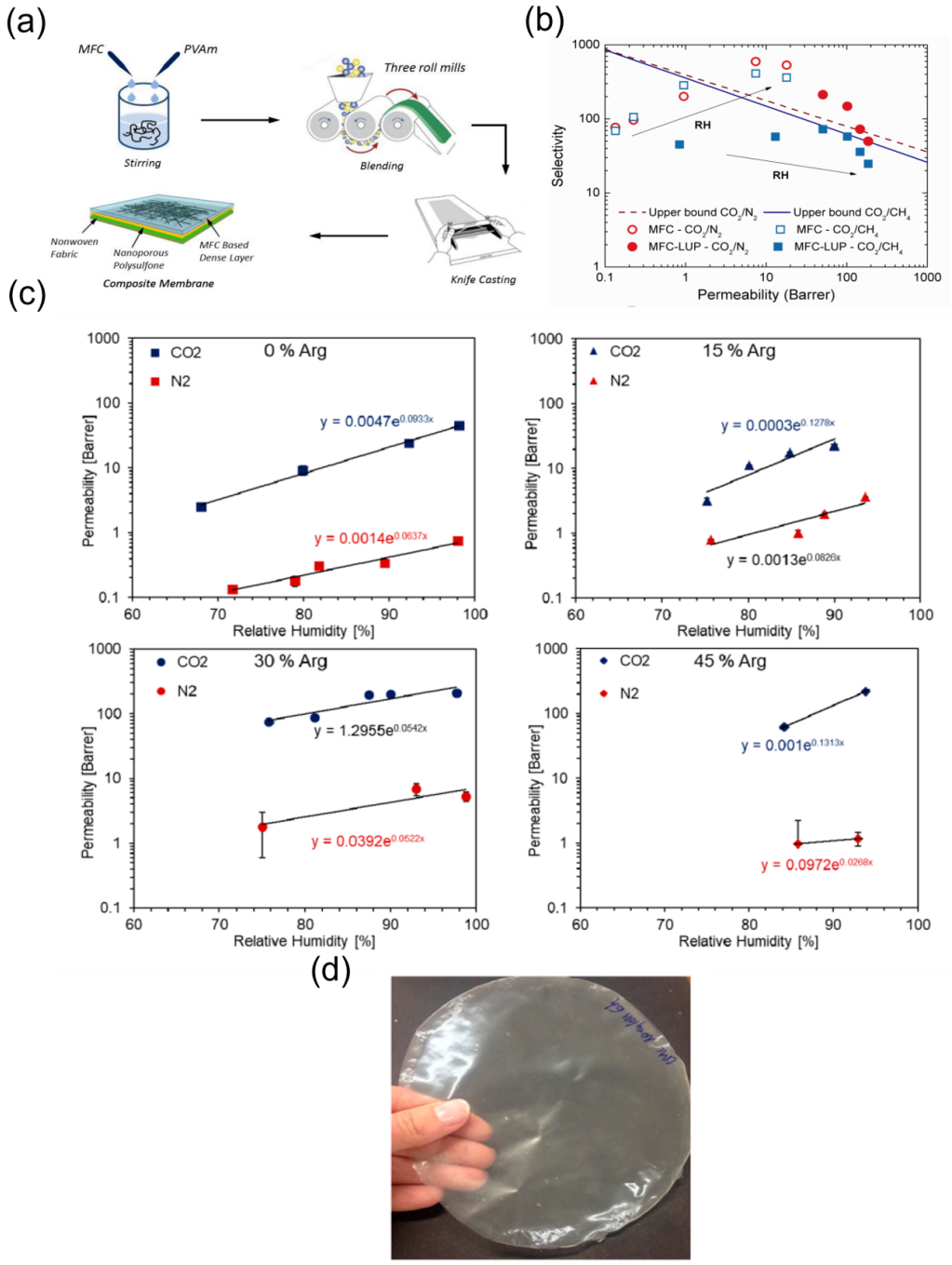

Figure 1. (**a**) Pictorial representation of generation of membranes. Reproduced with permission from [32]. (**b**) Graph showing selectivity vs. permeability of different materials. Reproduced with permission from [32]. (**c**) Single gas permeation results of CMC-NFC with different loadings of Arginine with respect to relative humidity. Reproduced with permission from [34]. (**d**) Membrane developed without arginine. Reproduced with permission from [34].

3.2. Chitosan

Natural biopolymer chitosan (CS) is a marine waste material that may be used in CO_2 adsorption because of its ease of processability, low maintenance and energy necessity. CS is inexpensive, abundantly available, renewable, environmentally friendly and biodegradable polysaccharide which is the second most abundant natural polysaccharide after cellulose [39]. CS chains have a large number of basic amine groups which facilitate adsorption of the acidic CO_2 molecule on the surface of the adsorbents [40,41]. However, pure chitosan suffers from low carbon dioxide adsorption due to the lower surface area thus most of the studies reporting chitosan-derived sorbents aim to fabricate the surface properties and maximize the CO_2 adsorption capacity [42]. Like cellulose materials, carbonization to chitosan-based materials has also resulted in efficient CO_2 adsorbent which are discussed herein. Hierarchical porous nitrogen-containing activated carbons (N-ACs) were prepared with LiCl-$ZnCl_2$ molten salt as a template derived from cheap chitosan via simple one-step carbonization under Ar atmosphere. The obtained N-ACs with the highest specific surface area of 2025 $m^2\ g^{-1}$ and a high nitrogen content of 5.1 wt% were obtained using a low molten salt/chitosan mass ratio (3/1) and moderate calcination temperature (1000 °C). Importantly, using these N-ACs as CO_2 solid-state adsorbents, the maximum CO_2 capture capacities could be up to 7.9/5.6 mmol g^{-1} at 0 °C/25 °C under 1 bar pressure, respectively. These CO_2 capture capacities of N-ACs were the highest compared to reported biomass-derived carbon materials, and these values were also comparable to most of porous carbon materials. Moreover, these N-ACs also showed good selectivity for CO_2/N_2 separation and excellent recyclability [43]. Chagas et al. reported a green method for CO_2 capture by showing the effects of hydrothermal carbonization (HTC) on chitosan's chemical properties and its potential. HTC allows changes in chitosan's surfaces and structural properties, increasing the CO_2 adsorption capacity by 4-fold compared to the non-HTC treated chitosan [44]. Kamaran et al. developed acetic acid-mediated chitosan-based porous carbons by a combination of hydrothermal carbonization treatment and chemical activation with KOH and NaOH under a flowing stream of nitrogen which developed. They noticed that would increase the CO_2 uptake to 8.36 mmol g^{-1} for KOH samples and 7.38 mmol g^{-1} for the NaOH sample. These synthesized carbon adsorbents also exhibited regenerability after four consecutive adsorption–desorption cycles and also high CO_2 capture selectivity over N_2 gas [45].

A non-carbonized chitosan–bleaching earth clay composite (Chi–BE) has been reported by Azharul Islam et al. as an efficient adsorbent for CO_2. They showed that temperature, adsorbent loading and CO_2 concentration exerted significantly positive effects on CO_2 adsorption by Chi–BE within the ranges and levels studied, whereas the interaction of adsorbent loading and CO_2 concentration only affected CO_2 adsorption. The optimised factors were 38.13 °C, adsorbent loading of 0.72 g and CO_2 concentration of 25%, which produced the adsorption capacity of 7.84 mmol g^{-1} using the desirability function which was very close to the validation study and the composite can also be recycled which shows its cost-effectiveness [46]. Material type and composition, BET surface area ($m^2\ g^{-1}$), pore size (nm)/total pore volume ($cm^3\ g^{-1}$), mechanism of adsorption, CO_2 capture capacity (mmol g^{-1}) and special features of chitosan-based materials have been tabulated in Table 2.

Table 2. Summary of material type and composition, BET surface area ($m^2\ g^{-1}$), pore size (nm)/total pore volume ($cm^3\ g^{-1}$), mechanism of adsorption, CO_2 capture capacity (mmol g^{-1}) and special features of chitosan-based materials.

Material Type and Composition	BET Surface Area ($m^2\ g^{-1}$)	Pore Size (nm)/Total Pore Volume ($cm^3\ g^{-1}$)	Mechanism of Adsorption	CO_2 Capture Capacity (mmol g^{-1})	Special Features	Ref
N-doped Atcivated carbon from chitosan char by KOH activation	907	0.39	Physisorption	1.86	High CO_2/N_2 selectivity and excellent recyclability	[40]

Table 2. *Cont.*

Material Type and Composition	BET Surface Area (m^2 g^{-1})	Pore Size (nm)/Total Pore Volume (cm^3 g^{-1})	Mechanism of Adsorption	CO_2 Capture Capacity (mmol g^{-1})	Special Features	Ref
N-doped carbonized chitosan	849	0.5–1.0 nm, 1.0–1.5 nm and 1.5–2.5 nm with maximum pore volume of 0.68	Physisorption	3.2	Can be used as an electrode material and adsorbent	[41]
Pyrolyzed chitosan- and chitosan-periodic mesoporous organosilica (PMO)-based porous materials	376	~2 nm, 0.346	Physisorption	1.9 at 500 kPa	Best selectivity for CO_2/CH_4 separation at 1.5% (m/v) of chitosan solution dried under supercritical CO_2	[42]
N containing activated carbons (N-ACs) with LiCl-$ZnCl_2$ molten salt as a template derived from cheap chitosan by carbonization.	2025	1.15	Physisorption	7.9 mmol g^{-1} at 0 °C/25 °C, 1 bar	Selectivity for CO_2/N_2 separation, excellent recyclability	[43]
Hydrothermal carbonized (HTC) of chitosan	2	-	Adsorption by the acid−base reaction between the CO_2 molecule and the basic sites of the materials, associated with the presence of nitrogen atoms	0.45	-	[44]
Acetic acid-mediated chitosan-based highly porous carbon adsorbents	4168	1.386	Physisorption	8.36	CO_2 selectivity over N_2	[45]
Chitosan-Bleaching earth	71.26	0.19	Physisorption	7.65	Recyclable	[46]

3.3. Lignin

Lignin is a class of complex organic polymers that form key structural materials in the support tissues of most plants. Lignins are particularly important in the formation of cell walls, especially in wood and bark. Chemically, lignins are polymers made by cross-linking phenolic precursors. Zhao et al. have reported the synthesis of multiscale carbonized carbon supraparticles (SPs) by soft-templating lignin nano- and microbeads bound with cellulose nanofibrils (CNFs) which were well suited for CO_2 capture (1.75 mmol g^{-1}), while presenting a relatively low pressure drop (~33 kPa·m^{-1} calculated for a packed fixed-bed column). Moreover, the carbon SPs did not require doping with heteroatoms for effective CO_2 uptake and also showed regeneration after multiple adsorption/desorption cycles [47]. While non-carbonized lignin-based materials have been reported by Shao et al. and Liu et al. [48,49]. They have reported lignin depolymerization selecting six aromatic units from lignin and developed O-rich hyper-cross-linked polymers (HCPs) by one-pot Friedel–Crafts alkylation reaction for CO_2 capture. Lignin-modified hyper-cross-linked nanoporous resins for efficient CO_2 capture have been described in a recent report. The resins were synthesized from lignin, 4-vinylbenzyl chloride, and divinylbenzene by free radical polymerization reaction followed by Friedel–Crafts reaction which displayed excellent CO_2 capture (1.96 mmol g^{-1}) at 273 K and 1 bar and reusability [49].

3.4. Cyclodextrins

Cyclodextrins are glucopyranosides bound together in various ring sizes renowned for their structural, physical and chemical properties. They are widely used in industrial applications due to their unique ability to encapsulate other molecules [50]. The

cyclodextrin (CD)/graphene composite aerogel synthesized by hydrothermal carbonized reaction at 80 °C for 18 h exhibits an adsorption capacity of CO_2 at 1.02 mmol g^{-1} [51]. Cyclodextrin-based non-carbonized materials have been also reported to be efficient CO_2 adsorbent [52–54]. Two isostructural cyclodextrin-based CD-MOFs (CD-MOF-1 and CD-MOF-2) are demonstrated to have an inverse ability to selectively capture CO_2 from C_2H_2 by single-component adsorption isotherms and dynamic breakthrough experiments. These two MOFs exhibit excellent adsorption capacity and benchmark selectivity (118.7) for CO_2/C_2H_2 mixture at room temperature [52]. In addition, a new solid acid adsorbent for CO_2 capture derived from β-cyclodextrin has been obtained and achieves a capacity of 39.87 cm^3/g at 3.5 bar [53]. For thermal activation, a rapid temperature-assisted synthesis has been reported to improve the porous structure of the cyclodextrins for CO_2 adsorption [54]. A third category of cyclodextrin-based materials involves CO_2 adsorption by thermal activation under N_2 atmosphere [55,56]. The adsorption thermodynamics of CO_2 on β-CD-derived adsorbent by thermal activation have been reported recently [55]. However, the pore formation mechanism during the thermal activation of β-CD for CO_2 uptake was systematically investigated by the same group in another study [56].

4. Synthetic Porous Organic Polymers (POPs) for CO_2 Capture

Synthetic porous organic polymers are a good choice of materials for post-combustion carbon dioxide capture because of their low density, high porosity, large surface area, and high stability. Various types of chemical reactions, such as Suzuki–Miyaura coupling, Sonogashira–Hagihara coupling, Buchwald–Hartwig amination, Schiff-base reaction, Friedel–Crafts reaction, etc., are used to synthesize organic polymers. The desired pore size of the polymers is obtained by selecting monomer building blocks and linkers. Affinity for CO_2 can also be enhanced by post-synthetic modification of the polymers. Various kinds of porous organic polymers have been reported in the literature. Out of them, hyper-crosslinked polymers (HCPs), covalent organic frameworks (COFs), conjugated microporous polymers (CMPs) and covalent triazine-based frameworks (CTFs) were used extensively for CO_2 capture [57]. Syntheses and CO_2 capture capacities of these four major types of POPs published in the last five years are summarised here. In Table 3, synthetic methods, measured parameters related to CO_2 capture, CO_2 capture capacities and CO_2/N_2 selectivities of the POPs mentioned in this review are shown.

4.1. Hyper-Crosslinked Polymers (HCPs)

Friedel–Crafts and simple condensation reactions are usually employed to prepare HCPs from monomers. Extensive cross-linking between the monomers creates permanent porosity in the HCPs. In general, HCPs displayed good CO_2 capture capacity though the surface area of the majority of these types of polymers is low. Hu et al. synthesized a microporous polymer, termed PIM-1, by one-step condensation of 5,5′,6,6′-tetrahydroxy-3,3,3′,3′-tetramethyl-1,1′-spirobisindane and 2,3,5,6-tetrafluoroterephthalonitrile. Hydrolysis of PIM-1 using NaOH produced the hydrolyzed form hPIM-1. Measured BET surface areas of the polymers were found to be 970 and 780 m^2/g for PIM-1 and hPIM-1, respectively. Hydrophilic hPIM-1 exhibited slightly higher CO_2 uptake capacity (1.73 mmol g^{-1} at 298 K and 1 bar) than that of PIM-1. Both polymers are also effective in the uptake of CO_2 at low partial pressure such as 0.15 bar. PIM-1 exhibited high competitive adsorption of CO_2 over N_2 at a high total pressure of 1 bar and a certain level of moisture resistance. PIM-1 can be solution-reprocessed keeping its CO_2 uptake capacity intact [58]. Fayemiwo et al. synthesized a series of nitrogen-rich HCPs, poly[methacrylamide-co-(ethylene glycol dimethacrylate)] by copolymerisation of methacrylamide (MAAM) and ethylene glycol dimethacrylate (EGDMA) in different molar ratio via radical initiated bulk polymerizations. Three polymers, termed HCP-MAAM-1, -2, -3 were obtained by increasing the concentrations of MAAM with respect to EGDMA by 1:2:3, respectively. These polymers exhibited high affinities towards CO_2 at both high and low pressure due to the presence of polar amide groups within the polymer network. CO_2 adsorption capacities were found to be 1.56, 1.45, and 1.28 mmol g^{-1} for HCP-MAAM-1, -2,

and -3, respectively, at 273 K and 1 bar. The reduction in the adsorption capacities with an increase in the concentration of MAAM with respect to EGDMA in the polymers is due to a decrease in the specific surface areas [59]. A series of hydroxyl-based HCPs was synthesized by Liu et al. via one-pot Friedel–Crafts alkylation of benzyl alcohol (BA) using formaldehyde dimethyl acetal (FDA) as external cross-linker and anhydrous $FeCl_3$. Pore volumes of the synthesized HCPs were found to be very sensitive to the reaction time and amounts of $FeCl_3$ and FDA. The HCPs obtained by use of optimized amounts of $FeCl_3$ and FDA in the reactions possess high BET-specific surface areas up to 1101 m^2/g and exhibit high CO_2 uptake capacities up to 3.03 mmol g^{-1} at 273 K and 1 bar [60]. Abdelnaby et al. synthesized an HCP, termed KFUPM-1, by acid-catalyzed condensation of pyrrole, 1,4-benzenediamine and p-formaldehyde. The presence of a high concentration of amine groups in the backbone of this meso-/macroporous polymer resulted in high selectivity (141) for CO_2 over N_2 and moderate CO_2 uptake capacity of 1.04 mmol g^{-1} at 298 K and 1 bar [61]. In a similar manner, another HCP, termed KFUPM-2, was synthesized by Friedel−Crafts alkylation polymerization of phenothiazine and pyrrole (1:3 ratio) using p-formaldehyde as a cross-linker in the presence of $FeCl_3$ as a catalyst. This microporous polymer showed a moderate CO_2 uptake capacity of 1.04 mmol g^{-1} with CO_2/N_2 selectivity of 51 at 298 K and 1 bar [62]. A novel ynone-linked porous organic polymer, named y-POP, was synthesized by Kong et al. by Sonogashira coupling of 1,3,5-triethynylbenzene with terephthaloyl chloride. Post-modification of y-POP by tethering alkyl amine species produced y-POP-NH_2. Increase in amine loading, the CO_2 adsorption capacity of y-POP-NH_2 gradually increased up to 1.95 mmol g^{-1} at 273 K and 1 bar from the corresponding value of 1.34 mmol g^{-1} of y-POP under the same conditions [63]. Cross-linking of a copolymer polydivinylbenzenechloride (PDV) was performed by reaction with anhydrous $FeCl_3$ and CCl_4 to produce methylene cross-linked HCP, named PDV-pc-1. Another carbonyl cross-linked HCP, named PDV-pc-2 was obtained in a similar reaction without using CCl_4. Studies showed that PDV-pc-1 has a higher BET-specific surface area (686 m^2/g) than PDV-pc-2 (635 m^2/g). However, the CO_2 uptake capacity of PDV-pc-2 (1.95 mmol g^{-1}) was found to be higher than PDV-pc-1 (1.45 mmol g^{-1}) at 273 K and 1 bar. Higher porosity and the presence of a large number of carbonyl functional groups made PDV-pc-2 a better CO_2-capturing agent [64]. Sharma et al. synthesized a heptazine-based microporous polymeric network, termed HMP-TAPA, by nucleophilic substitution of trichloroheptazine (TCH) by tris-(4-aminopenyl) amine (TAPA). The presence of a large number of CO_2-philic -N-, -NH, and -NH_2 groups on the surface enhanced CO_2 sorption capacity of HMP-TAPA, which exhibited a CO_2 uptake capacity of 2.42 mmol g^{-1} at 273 K and 1 bar. In addition, this polymer catalyzed the cycloaddition of CO_2 with epoxides under mild conditions to generate cyclic carbonates with high yield and selectivity [65]. A series of N-containing HCPs was synthesized from triphenylamine (TPA) and/or carbazole (Cz) monomers by one-step cross-coupling reactions including Scholl coupling and solvent knitting Friedel–Crafts reactions. Among these microporous polymers, HCP1, HCP2, and HCP3, prepared by Scholl coupling exhibited high CO_2 uptake capacities (2.38–2.64 mmol g^{-1} at 273 K and 1 bar) due to high porosity though measured surface areas were found to be low. On the other hand, HCP4, HCP5, and HCP6, prepared by 1,2-dichloroethane knitting Friedel–Crafts reactions were found to be meso/macroporous in nature and they exhibited comparatively low CO_2 uptake capacities (0.9–1.52 mmol g^{-1} at 273 K and 1 bar) due to their low porosity [66]. Mohamed et al. synthesized two microporous HCPs, named TPE-CPOP1 and TPE-CPOP2, by $AlCl_3$ catalysed Friedel–Crafts reactions of tetraphenylethene (TPE) monomer with and without cyanuric chloride, respectively. CO_2 adsorption capacities were found to be 0.89 and 1.15 mmol g^{-1} at 298 K and 1 bar for TPE-CPOP1 and TPE-CPOP2, respectively. Higher CO_2 uptake capacity of TPE-CPOP2 is caused by the presence of triazine units in the framework. The carbonization and KOH activation process of these HCPs produced porous carbon materials which exhibited high CO_2 uptake capacities (Figure 2a) [67]. Qiao et al. prepared two HCPs, named P0 and P1, by one-step reaction of each p-terphenyl and 4-amino-p-terphenyl monomers with $AlCl_3$ catalyst in dichlorometane, respectively.

Further reaction of nitrobenzene and P1 in 1:3 ratios afforded another HCP, named P2. CO_2 uptake capacities of P0, P1 and P2 were found to be 3.79, 4.24, and 3.02 mmol g^{-1} at 273 K and 1.13 bar. The remarkable CO_2 uptake capacity of P1 was attributed due to the presence of the amine groups in the polymeric network [68]. Zhou et al. synthesized a series of microporous HCPs by Friedel−Crafts polymerization of each hexaphenylbenzene (HPB), triphenylbenzene (TPB), spirobisfluorene (SBF), and triptycene (Trip) monomers catalyzed by $AlCl_3$ in the presence of dichloromethane, which acts as both the solvent and as a cross-linker. The polymers were functionalized further by covalently attaching $-NO_2$, $-NH_2$, and $-SO_3H$ groups. Generally, surface functionalization of the polymers causes loss of porosity but nitro- and sulfonic acid-containing polymers retained a good amount of initial porosity. Sulfonated polymers showed high BET surface areas in the range of 1145 to 1390 m^2/g and highest CO_2 uptake capacity reached to 6.77 mmol g^{-1} at 273 K and 1 bar [69]. Abdelnaby et al. synthesized two azo-linked porous organic polymers, termed man-Azo-P1 and man-Azo-P2, by diazotization reactions of 4,4′-diaminobiphenyl (benzidine) and 4,4′-diaminodianiline, respectively, with phloroglucinol in aqueous medium at 0 °C. The CO_2 uptake capacities were found to be 1.43 and 0.89 mmol g^{-1} at 273 K and 1 bar for man-Azo-P1 and man-Azo-P2, respectively. The former exhibited better CO_2 uptake capacity due to the presence of polar azo and hydroxy functional groups in the framework [70].

4.2. Covalent Organic Frameworks (COFs)

Precise control of the structure and pore size of COFs is performed by choosing the monomer building blocks and reaction conditions. Gao et al. synthesized two 2D-COFs by condensation of amine and aldehyde functionalized tetraphenylethane (TPE). Solvent controlled [4 + 4] condensation produced TPE-COF-I and an unusual [2 + 4] condensation pathway produced TPE-COF-II. TPE-COF-II exhibited higher CO_2 capture capacity (5.3 mmol g^{-1} at 273 K and 1 atm) than TPE-COF-I (3.06 mmol g^{-1}) due to the presence of unreacted-CHO groups in the framework [71]. Li et al. designed and synthesized a metalloporphyrin-containing COF by solvothermal reaction of cobalt(II)-5,10,15,20-tetrakis(4-aminophenyl)porphyrin (Co(II)@TAPP) and tetrakis(4-formylphenyl)pyrene (TFPPy). The COF captures CO_2 and catalytically converts it into cyclic carbonates under mild conditions. BET surface area of the microporous COF was found to be 1076 m^2/g and the pore size was 1.6 nm. High surface area, good stability and the presence of a single type of micropores made it a good catalyst. The COF exhibited a strong CO_2 adsorption capacity of 3.84 mmol g^{-1} (16.9 wt%) at 298 K and 1 bar. Co(II)@TAPP units in the COF are alternately stacked perpendicular to the porphyrin planes with a slipped distance of 1.7 Å which fits with the size of CO_2. Adsorbed CO_2 molecules interact effectively with the metal centres (catalytic sites) and facilitate catalytic reactions (Figure 2b) [72]. Lyu et al. established a new synthetic strategy to covalently attach aliphatic amines to construct COFs. First, an imine-linked COF, named COF-609-Im, was synthesized through imine condensation between 2,4,6-tris(4-formylphenyl)-1,3,5-triazine (TFPT) and 4,4′-diaminobenzanilide (DABA). Crystallization of COF-609-Im, followed by conversion of its imine linkage to base-stable tetrahydroquinoline (THQ) linkage through aza-Diels−Alder cycloaddition produced COF-609-THQ-Im. Finally, the covalent incorporation of tris(3-aminopropyl)amine (TRPN) into the framework produced COF-609. All three COFs are porous amorphous in nature and the BET surface area of COF-609-Im was found to be 724 m^2/g. CO_2 capture capacity of COF-609 was found to be 6.8 cm^3/g (0.304 mmol g^{-1}) which is 1360 times higher compared to that of COF-609-THQ-Im at 0.4 mbar CO_2 at 273 K. Further 29% increase in CO_2 capture was observed in the presence of humidity. This condition is comparable to direct air capture of CO_2. Strong chemisorptions of CO_2 by aliphatic amines incorporated into COFs made these sorbents such efficient capturing agents at low CO_2 pressures. These three COFs also exhibited excellent CO_2 capture capacities at 40 mbar (comparable to post-combustion capture from natural gas burned flue gas) and 150 mbar (comparable to post-combustion capture from coal-fired flue gas) pressures of CO_2 [73].

4.3. Conjugated Microporous Polymers (CMPs)

Usually, CMPs are prepared by coupling/cross-coupling reactions of aromatic monomers by many well-known reactions, such as, Suzuki, Sonogashira, Yamamoto cross-coupling reactions. Pore size, surface areas and CO_2-philic nature of the polymers can be tuned by proper selection of monomers, reaction type and post-synthetic modifications [74]. Wang et al. synthesized three novel biphenylene-based CMPs, termed CMP-LS1, CMP-LS2 and CMP-LS3, by palladium-catalyzed Suzuki and Sonogashira–Hagihara cross-coupling reactions of 3,4′,5-tribromobiphenyl (TBBP) with each 1,4-phenylenediboronic acid, 1,3,5-tris(4,4,5,5-tetramethyl-1,3,2-dioxaborolan-2-yl)benzene and 1,3,5-triethynylbenzene, respectively. BET surface areas of these porous polymers were found to be 493, 1576 and 643 cm^2/g for CMP-LS1, CMP-LS2 and CMP-LS3, respectively. Among the three CMPs, CMP-LS2 exhibited highest CO_2 adsorption capacity of 3.88 mmol g^{-1} at 273 K and 1 bar due to its large surface area [75]. By oxidative homocoupling of 1,3,6,8-tetraethynylpyrene monomer using Pd(II)-Cu(I) catalysts Ren et al. prepared a CMP, named LKK-CMP-1. This 1,3-diyne linked CMP exhibited moderate CO_2 uptake capacity (2.22 mmol g^{-1} at 273 K and 1 bar) (Figure 2c) [76]. Saber et al. synthesized two azo-linked CMPs, termed Azo-Cz-CMP and Azo-Tz-CMP, by reduction of the corresponding monomers 3,6-dinitro-9-(4-nitrophenyl) carbazole (Cz-3NO_2) and 3,7-dinitro-10-(4-nitrophenyl)-10H-phenothiazine (Tz-3NO_2), respectively, using sodium borohydride ($NaBH_4$). BET surface areas of both CMPs were found to be low and pore sizes centered at 0.79 and 1.18 nm for Azo-Cz-CMP and Azo-Tz-CMP, respectively. The former exhibited higher CO_2 capture value of 2.13 mmol g^{-1} at 298 K and 1 bar than the later which showed 1.36 mmol g^{-1} CO_2 capture capacity under same conditions [77].

Table 3. Summary of synthetic process, surface area, pore size, total pore volume, CO_2 uptake capacity, CO_2/N_2 selectivity and heat of adsorption of the synthetic POPs.

POPs	Synthetic Process	S_{BET} [a]	Pore Size [b]	V_{tot} [c]	CO_2 Capture Capacity [d]		CO_2/N_2 Selectivity [e]		Q_{st} [f]	Ref.
					273 K	298 K	273 K	298 K		
PIM-1	One-step condensation in presence of K_2CO_3	970	<2, 2–50	0.70	-	1.66	-	19.3	20.8	[58]
hPIM-1	Hydrolyzation of PIM-1 using NaOH	780	<2, 2–50	0.49	-	1.73	-	11.7	32.8	[58]
HCP-MAAM-1	Radical initiated bulk copolymerization	298	2–40	0.47	1.56	0.92	45–86	38–48	28–35	[59]
HCP-MAAM-2	Radical initiated bulk copolymerization	142	2–40	0.87	1.45	0.85	50–99	38–63	28–35	[59]
HCP-MAAM-3	Radical initiated bulk copolymerization	83	2–40	0.24	1.28	0.79	52–104	45–72	28–35	[59]
BAHCP-7	Friedel-Crafts alkylation polymerization	1101	1.7	1.15	3.03	1.96	35	-	26–28	[60]
KFUPM-1	Acid catalyzed polycondensation	305	-	-	1.52	1.04	-	141	34	[61]
KFUPM-2	Friedel−Crafts alkylation polymerization	352	-	0.21	1.75	1.04	-	51	34	[62]
y-POP	Sonogashira coupling	226	0.74, 1.2, 34	-	1.34	-	20	-	29	[63]
y-POP-A1	Amine modification of y-POP	145	-	-	1.50	-	239	-	46.8	[63]
PDV	Radical polymerzation	364	1–2	0.20	0.66	0.25	31.3	-	36.9	[64]
PDV-pc-1	Friedel−Crafts reaction of PDV	686	1–2	0.37	1.45	0.59	16.4	-	34.3	[64]
PDV-pc-2	Friedel−Crafts reaction of PDV	635	1–2	0.33	1.95	0.80	46.8	-	39.7	[64]

Table 3. *Cont.*

POPs	Synthetic Process	S_{BET} [a]	Pore Size [b]	V_{tot} [c]	CO_2 Capture Capacity [d]		CO_2/N_2 Selectivity [e]		Q_{st} [f]	Ref.
					273 K	298 K	273 K	298 K		
HMP-TAPA	Polymerization via nucleophilic substitution reaction	424	0.7–1.2, 2–4	-	2.42	-	26.27	30.79	32.8	[65]
HCP1	Scholl coupling	534.5	-	0.32	2.64	1.57	23.6	-	46.7	[66]
HCP2	Scholl coupling	215.7	-	0.11	2.38	1.51	30.2	-	28.0	[66]
HCP3	Scholl coupling	199.9	-	0.12	2.47	1.46	26.7	-	36.7	[66]
HCP4	Friedel−Crafts alkylation polymerization	10.8	-	0.023	1.05	0.72	8.6	-	26.2	[66]
HCP5	Friedel−Crafts alkylation polymerization	34.8	-	0.065	1.52	0.72	15.4	-	39.8	[66]
HCP6	Friedel−Crafts alkylation polymerization	30.3	-	0.061	0.90	0.42	7.0	-	33.0	[66]
TPE-CPOP1	Friedel-Crafts polymerization	489	1.49, 1.82	0.269	0.99	0.89	-	-	-	[67]
TPE-CPOP2	Friedel-Crafts polymerization	146	2.57	0.1	1.26	1.15	-	-	-	[67]
TPE-CPOP1-800	Carbonization and KOH activation of TPE-CPOP1	1177	1.04, 2.99	0.48	3.19	1.74	-	-	-	[67]
TPE-CPOP2-800	Carbonization and KOH activation of TPE-CPOP2	1165	1.02, 2.29	0.62	2.93	1.72	-	-	-	[67]
P0	Friedel-Crafts polymerization	1062	5.65	0.69	3.79	-	-	18.28	24–32	[68]
P1	Friedel-Crafts polymerization	447	1.91	0.21	4.24	-	-	20.97	24–32	[68]
P2	Condensation polymerization using base	242	1.94	0.12	3.02	-	-	34.52	24–32	[68]
PIM-TPB	Friedel−Crafts polymerization	2540	0.35, 0.56, 0.86	1.300	5.00	2.57	-	14.1	25.2	[69]
PIM-TPB-NO_2	-NO_2 functionalization of PIM-TPB using HNO_3	950	0.35, 0.56, 0.86	0.553	5.13	3.11	-	24.7	32.1	[69]
PIM-TPB-NH_2	-NH_2 functionalization by $Na_2S_2O_4$ treatment of PIM-TPB-NO_2	710	0.35, 0.56, 0.86	0.333	4.45	2.98	-	26.1	31.7	[69]
PIM-TPB-HSO_3	-SO_3H functionalization of PIM-TPB using H_2SO_4	1585	0.35, 0.56, 0.86	0.852	6.77	4.07	-	17.9	29.0	[69]
man-Azo-P1	Diazotization of aromatic diamines followed by coupling with aromatic alcohol	290	-	0.33	1.43	-	80	-	40	[70]
man-Azo-P2	Diazotization of aromatic diamines followed by coupling with aromatic alcohol	78	-	0.15	0.89	-	110	-	23	[70]
TPE-COF-I	Acid catalysed condensation	1535	-	1.65	3.06	1.69	-	-	-	[71]
TPE-COF-II	Acid catalysed condensation	2168	-	2.14	5.30	2.70	-	-	-	[71]
Co(II)@TA-TF COF	Solvothermal reaction	1076	1.6	-	-	3.84	-	-	-	[72]
COF-609-Im	Acid catalysed condensation	724	-	-	1.5	-	-	-	-	[73]
COF-609	aza-Diels−Alder cycloaddition of COF-609-Im followed by amination	-	-	-	0.076	-	-	-	-	[73]

Table 3. *Cont.*

POPs	Synthetic Process	S_{BET} [a]	Pore Size [b]	V_{tot} [c]	CO_2 Capture Capacity [d]		CO_2/N_2 Selectivity [e]		Q_{st} [f]	Ref.
					273 K	298 K	273 K	298 K		
CMP-LS1	Suzuki coupling	493	0.4–1.4	0.32	1.38	0.76	23.2	-	30.2	[75]
CMP-LS2	Suzuki coupling	1576	0.4–1.4	1.06	3.88	2.1	27.9	-	31.6	[75]
CMP-LS3	Sonogashira-Hagihara coupling	643	0.4–1.4	0.37	1.88	1.07	19.8	-	30.4	[75]
LKK-CMP-1	Oxidative homocoupling	467	0.59	0.371	2.22	1.38	-	44.2	35	[76]
Azo-Cz-CMP	One-pot reductive reaction using $NABH_4$	315	0.79	-	2.13	0.91	-	-	32.08	[77]
Azo-Tz-CMP	One-pot reductive reaction using $NABH_4$	225	1.18	-	1.36	0.64	-	-	18.36	[77]
TrzPOP-1	Polycondensation	995	1.7	-	6.19	3.53	108.4	42.1	29	[78]
TrzPOP-2	Polycondensation	868	1.5	-	7.51	4.52	140.6	75.7	34	[78]
TrzPOP-3	Polycondensation	772	1.4	-	8.54	5.09	167.4	94.5	37	[78]
NT-POP-5	Suzuki cross-coupling	8	-	-	0.78	-	-	-	25.4–19.4	[79]
NT-POP@800-4	Pyrolysis of NT-POP-1-6 at 800 °C	736	-	0.463	3.96	3.25	36.9	-	25.4–19.4	[79]
CTF1	$ZnCl_2$ catalyzed ionothermal reaction	1654	-	1.06	5.23	3.32	-	11	34.0	[80]
CTF4	$ZnCl_2$ catalyzed ionothermal reaction	784	-	0.41	4.39	3.83	-	46	21.5	[80]
CTF-DCE	$ZnCl_2$ catalyzed ionothermal reaction	1355	0.6, 1.2, 2–4	0.93	4.34	3.59	54	-	24.9	[81]
CTF-PF-4	$ZnCl_2$ catalyzed ionothermal reaction	889	1.7–1.9	0.58	2.0	1.27	-	-	>33	[82]
ICTF-Cl	$ZnCl_2$ catalyzed ionothermal reaction	751	-	0.458 (approx.)	2.36	1.41	119.1	68.74	-	[83]
ICTF-SCN	$ZnCl_2$ catalyzed ionothermal reaction	1000 (approx.)	-	0.458 (approx.)	2.48	1.40	39.28	24.82	-	[83]
CTF-N4	$ZnCl_2$-mediated cyclotrimerization	701	-	0.31	3.4	2.2	45	-	44	[84]
CTF-N6	$ZnCl_2$-mediated cyclotrimerization at high temperature	1236	-	0.51	5.0	3.4	36	-	26	[84]
CTF-hex4	$ZnCl_2$-mediated ionothermal reaction	609	-	0.31	3.4	-	-	-	29	[85]
CTF-hex6	$ZnCl_2$-mediated ionothermal reaction	1728	-	0.87	3.1	-	-	-	37	[85]
An-CTF-20-500	$ZnCl_2$-mediated ionothermal reaction	700	1.06, 1.66	-	5.25	2.69	-	-	-	[86]

[a] BET surface area ($m^2\ g^{-1}$). [b] Pore size (nm). [c] Total pore volume ($cm^3\ g^{-1}$). [d] CO_2 capture capacity (mmol g^{-1}) at 1 bar. [e] IAST (ideal adsorbed solution theory) for the mixture including 85% of N_2 and 15% of CO_2 at 1 bar. [f] Heat of absorption (kJ mol^{-1}) of CO_2 (calculated using Clausius-Clapeyron equation at low CO_2 loading).

4.4. Covalent Triazine-Based Frameworks (CTFs)

High nitrogen content of the aromatic triazine (C_3N_3) rings in the CTFs enhances affinity for CO_2. Furthermore, high stability and abundant micropores in the surface made CTFs potential CO_2 capturing agents [5]. Das et al. synthesized three CTFs, namely TrzPOP-1, -2 and -3, via polycondensation of two tetraamine bearing triazine ring and three different dialdehydes (two of them contain phenolic –OH groups). TrzPOP-1, -2 and -3

possess high BET surface areas of 995, 868 and 772 m^2/g, respectively, and they exhibited high CO_2 uptake capacities of 6.19, 7.51 and 8.54 mmol g^{-1}, respectively, at 273 K and 1 bar. Though BET surface areas of TrzPOP-2 and TrzPOP-3 are comparatively low still they exhibited high CO_2 uptakes because of the presence of phenolic –OH groups [78]. Yao et al. synthesized a series of six CTFs, termed NTPOP-1 to -6, by Suzuki cross-coupling driven polycondensation of N2, N4, N6-tris(4-bromophenyl)-1,3,5-triazine-2,4,6-triamine (TPTT) and a number of benzeneboronic monomers or ethynyl monomers. BET surface areas of the NTPOPs were found to be in the lower side and highest CO_2 uptake was 0.78 mmol g^{-1} at 273 K and 1.05 bar. Carbonization of these NTPOPs at 800 °C produced pore-tunable porous carbon materials which exhibited excellent CO_2 adsorption capacity of 2.83–3.96 mmol g^{-1} at 273 K and 1.05 bar [79]. A set of five CTFs (CTF1–5) were prepared by ionothermal reactions of dicyano-aryl or heteroaryl monomer and molten $ZnCl_2$ in 1:5 molar ratio at temperature 400 °C (first 10 h) and 600 °C (next 10 h). Obtained CTFs were found to be bimodal micro-mesoporous in nature and they displayed high specific surface areas (up to 1860 m^2/g). Selected polymers of this series displayed excellent CO_2 uptake and highest uptake value was found to be 5.23 and 3.83 mmol g^{-1} at 273 and 298 K, respectively, at ambient pressure [80]. In a similar way, Dang et al. synthesized a CTF, termed CTF-DCE, via $ZnCl_2$ catalyzed ionothermal trimerization of di(4-cyanophenyl)ethyne. CTF-DCE displayed high BET surface area of 1355 m^2/g and excellent CO_2 capture capacity of 4.34 mmol g^{-1} at 273 K and 1 bar [81]. Utilizing the similar strategy, a series of four CTFs based on imidazolium salts were synthesized by Xu et al. via ionothermal reactions of nitriles and $ZnCl_2$ in different ratios at 400 °C. The obtained CTFs, were termed as CTF-Cl-1, CTF-Cl-2, CTF-PF-3, and CTF-PF-4 based on the type and number of counterions (Cl^- and $PF_6{}^-$) present. These CTFs displayed high BET surface areas. Pore volumes and sizes of the CTFs can be controlled by simply exchange of counterions. CTF-PF-4 containing highest $PF_6{}^-$ content, showed highest CO_2 adsorption of 2.0 mmol g^{-1} [82]. Zhu et al. reported synthesis of a series of bipyridinium-based ionic covalent triazine frameworks (ICTFs) with anions Cl^- and SCN^- through $ZnCl_2$ catalyzed ionothermal polymerization. High specific surface area, microporous structure, ionic nature and high nitrogen content made them excellent CO_2 capturing agents. The surface area and porosity can be regulated by adjusting the anions. Both ICTF-SCN and ICTF-Cl showed high CO_2 uptake capacities of 2.48 and 2.36 mmol g^{-1} at 273 K and 1 bar, respectively [83]. Three PhNH-, PhO-, and PhS-linked CTFs were synthesized by Liao et al. via $ZnCl_2$ mediated cyclotrimerization of nitrile-containing monomers including 2,4,6-tris(4-cyanophenylamino)-1,3,5-triazine (TAT), 2,4,6-tris(4-cyanophenoxy)-1,3,5-triazine (TOT), and 2,4,6-tris(4-cyanobenzenesulfenyl)-1,3,5-triazine (TST) by stepwise heating method. These microporous CTFs possess high BET surface areas and found to be excellent CO_2 sorbents. The PhNH-linked CTF prepared at high temperature (600 °C) displayed very high CO_2 adsorption capacity (5.0 mmol g^{-1} at 273 K and 1 bar). The CO_2 capture performances of the three CTFs were found to be in the order of PhNH- > PhO- > PhS-linked CTF [84]. Wessely et al. reported synthesis of a series of CTFs using pseudo-octahedral hexanitrile 1,4-bis(tris(4′-cyanophenyl) methyl) benzene (BTB-nitrile) monomer. Among these, CTF-hex6 was prepared under ionothermal reaction conditions with $ZnCl_2$ at 400 °C and CTF-hex1 was prepared under mild reaction conditions with the strong Brønsted acid trifluoromethanesulfonic acid at room temperature. In addition, the BTB-nitrile was combined with different di-, tri-, and tetranitriles as a second linker under ionothermal reactions under the same conditions produced mixed-linker CTFs, named CTF-hex2-6. These CTFs displayed BET surface areas in a wide range of 493 m^2/g to 1728 m^2/g. They exhibited CO_2 capture capacities in the range 2.5 to 3.4 mmol g^{-1} at 273 K and 1 bar (Figure 2d) [85]. A series of porous covalent triazine framework (An-CTFs) based on 9,10 dicyanoanthracene (An-CN) units was prepared by Mohamed et al. via ionothermal reactions of AnCN and molten $ZnCl_2$ in two different molar ratios (1:10 and 1:20) at two different temperatures (400 °C and 500 °C). These microporous highly stable An-CTFs possessing moderate BET surface areas ranging from 406 to 751 m^2/g exhibited high CO_2 adsorption capacity up to 5.65 mmol g^{-1} at 273 K and 1 bar [86].

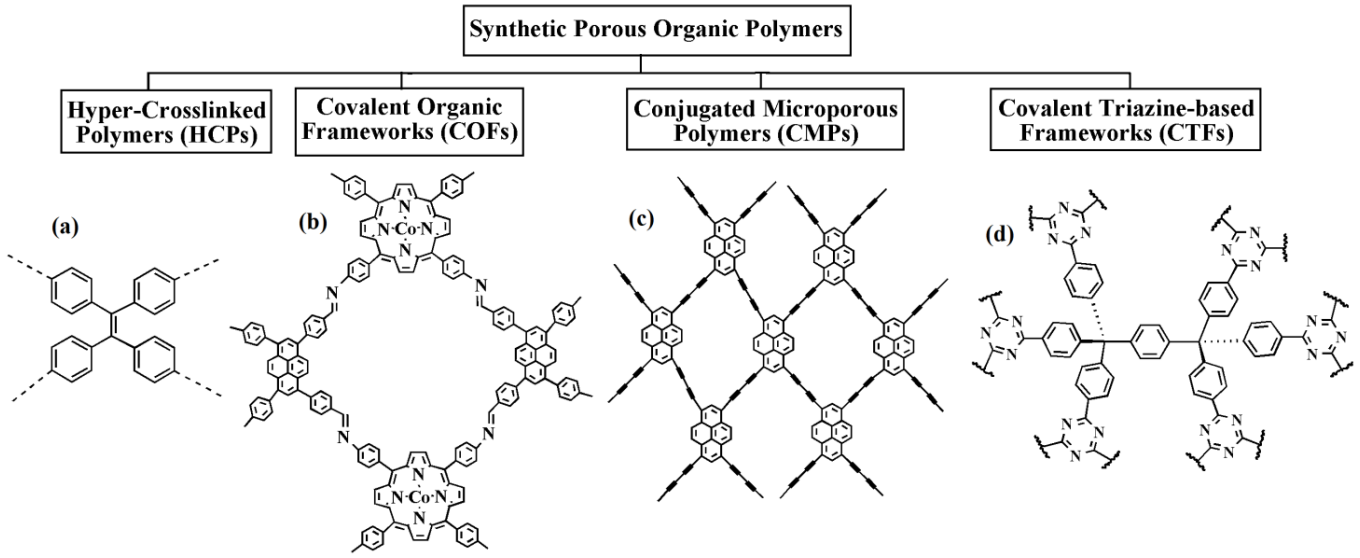

Figure 2. Types of synthetic porous organic polymers (POPs) with selected examples: (**a**) TPE-CPOP1. Adapted with permission from [67]. (**b**) Co(II) @ TA-TF COF. Adapted with permission from [72]. (**c**) LKK-CMP-1. Adapted with permission from [76]. (**d**) CTF-hex1–6. Adapted with permission from [85].

5. Conclusions and Outlook

In this review, we have summarized synthesis, CO_2 capture capacities and influential factors behind the CO_2-philicity of some novel natural and synthetic POPs reported in the literature in the last five years. Though CO_2 capture capacities of biopolymers are generally low but microporous and nanoporous materials derived from them exhibited superior adsorption capacity. Particularly, nanocellulose-based membranes were found to be potential candidates for large-scale capture of CO_2 and separation from flue gas. On average, synthetic POPs including HCPs, COFs, CMPs and CTFs showed higher CO_2 uptake capacity and selectivity than porous carbonaceous materials. POPs played a major role in the research of developing new materials for post-combustion CO_2 capture and separation. In general, POPs with high surface area (>1000 m^2/g), micropore, and presence of CO_2-philic functional groups (such as -NH_2, -OH, etc.) on the surface are proven to be promising candidates for CO_2 capture. A potential solid adsorbent for large-scale CO_2 capture should show >2 mmol g^{-1} CO_2 uptake, >100 CO_2/N_2 selectivity and good moisture resistivity. At the same time, large-scale production of the adsorbent must be cost-effective.

Although good progress has been achieved so far in CO_2 capture using POPs, there are still a lot of challenges. The limited solubility of many biopolymers (cellulose, chitin, lignin, etc.) in common solvents hinders surface modification and processability. As a result, difficulties arise in the preparation of POPs membranes which are highly useful for large-scale CO_2 uptake and separation. Many POPs were synthesized using costly monomers and metal catalysts which is a concern for their large-scale applications. The partial pressure of CO_2 in flue gas is as low as 3–15 kPa and the temperature is in the range of 80–90 °C. Hence, the CO_2 capture capacities of POPs at low pressure and high temperature should be improved.

The development of new-generation CO_2 capture materials with POPs and biopolymers requires fine-tuning the thermodynamics of the interaction between CO_2 and the adsorbent to improve the energy efficiency of CO_2 capture. In most cases, the CO_2 capture efficiency of the adsorbents was evaluated by single-component CO_2 uptake isotherms or breakthrough experiments using a CO_2/N_2 mixed gas. The presence of other minor gases (O_2, CO, SO_x, NO_x) and water vapour in the flue gas may have significant consequences on the performance of the materials. This issue must be taken into account during the

development of new-generation adsorbents. To decrease the cost of scaling up the materials for industrial applications new building blocks, synthetic routes and simple ways of post-functionalization should be explored. To improve the CO_2 capture capacities of POPs a lot of effort has already been made. The very fast progress in this field of research strongly indicates that synthetic and biopolymer-based materials will play a major role in developing next-generation CO_2 capturing agents to achieve the sustainable development goals (SDGs).

Author Contributions: Conceptualization, S.K.G. and M.G.; writing—original draft preparation, S.K.G. and M.G.; writing—review and editing, S.K.G. and M.G. All authors have read and agreed to the published version of the manuscript.

Funding: This research received no external funding.

Institutional Review Board Statement: Not applicable.

Conflicts of Interest: The authors declare no conflict of interest.

References

1. Raupach, M.R.; Marland, G.; Ciais, P.; Quẻré, C.L.; Canadell, J.G.; Klepper, G.; Field, C.B. Global and Regional Drivers of Accelerating CO_2 Emissions. *Proc. Natl. Acad. Sci. USA* **2007**, *104*, 10288–10293. [CrossRef] [PubMed]
2. Goeppert, A.; Czaun, M.; Prakash, G.K.S.; Olah, G.A. Air as the Renewable Carbon Source of the Future: An Overview of CO_2 Capture from the Atmosphere. *Energy Environ. Sci.* **2012**, *5*, 7833–7853. [CrossRef]
3. Qaroush, A.K.; Alshamaly, H.S.; Alazzeh, S.S.; Abeskhron, R.H.; Assaf, K.I.; Eftaiha, A.F. Inedible Saccharides: A Platform for CO_2 Capturing. *Chem. Sci.* **2018**, *9*, 1088–1100. [CrossRef] [PubMed]
4. Zeng, Y.; Zou, R.; Zhao, Y. Covalent Organic Frameworks for CO_2 Capture. *Adv. Mater.* **2016**, *28*, 2855–2873. [CrossRef]
5. Wang, W.; Zhou, M.; Yuan, D. Carbon Dioxide Capture in Amorphous Porous Organic Polymers. *J. Mater. Chem. A* **2017**, *5*, 1334–1347. [CrossRef]
6. Bhanja, P.; Modak, A.; Bhaumik, A. Porous Organic Polymers for CO_2 Storage and Conversion Reactions. *ChemCatChem* **2019**, *11*, 244–257. [CrossRef]
7. Ben-Mansour, R.; Habib, M.A.; Bamidele, O.E.; Basha, M.; Qasem, N.A.A.; Peedikakkal, A.; Laoui, T.; Ali, M. Carbon Capture by Physical Adsorption: Materials, Experimental Investigations and Numerical Modeling and Simulations: A Review. *Appl. Energy* **2016**, *161*, 225–255. [CrossRef]
8. Zou, L.; Sun, Y.; Che, S.; Yang, X.; Wang, X.; Bosch, M.; Wang, Q.; Li, H.; Smith, M.; Yuan, S.; et al. Porous Organic Polymers for Post-Combustion Carbon Capture. *Adv. Mater.* **2017**, *29*, 1700229. [CrossRef] [PubMed]
9. Porta, R.; Sabbah, M.; Di Pierro, P. Biopolymers as Food Packaging Materials. *Int. J. Mol. Sci.* **2020**, *21*, 4942. [CrossRef]
10. Inostroza-Brito, K.E.; Collin, E.C.; Majkowska, A.; Elsharkawy, S.; Rice, A.; Hernández, A.E.R.; Xiao, X.; Rodríguez-Cabello, J.C.; Mata, A. Cross-Linking of a Biopolymer-Peptide Co-assembling System. *Acta Biomater.* **2017**, *58*, 80–89. [CrossRef]
11. Ma, J.; Sahai, Y. Chitosan Biopolymer for Fuel Cell Applications. *Carbohydr. Polym.* **2013**, *92*, 955–975. [CrossRef]
12. Ghosh, M.; Majkowska, A.; Mirsa, R.; Bera, S.; Rodríguez-Cabello, J.C.; Mata, A.; Adler-Abramovich, L. Disordered Protein Stabilization by Co-Assembly of Short Peptides Enables Formation of Robust Membranes. *ACS Appl. Mater. Interfaces* **2022**, *14*, 464–473. [CrossRef] [PubMed]
13. Wu, J.; Shaidani, S.; Theodossiou, S.K.; Hartzell, E.J.; Kaplan, D.L. Localized, on-Demand, Sustained Drug Delivery from Biopolymer-Based Materials. *Expert Opin. Drug Deliv.* **2022**, *19*, 1317–1335. [CrossRef] [PubMed]
14. Ghosh, M.; Halperin-Sternfeld, M.; Grinberg, I.; Adler-Abramovich, L. Injectable Alginate-Peptide Composite Hydrogel as a Scaffold for Bone Tissue Regeneration. *Nanomaterials* **2019**, *9*, 497. [CrossRef]
15. Souza, M.A.D.; Vilas-Boas, I.T.; Leite-da-Silva, J.M.; Abrahão, P.D.N.; Teixeira-Costa, B.E.; Veiga-Junior, V.F. Polysaccharides in Agro-Industrial Biomass Residues. *Polysaccharides* **2022**, *3*, 95–120. [CrossRef]
16. Chowdhuri, S.; Ghosh, M.; Adler-Abramovich, L.; Das, D. The Effects of a Short Self-Assembling Peptide on the Physical and Biological Properties of Biopolymer Hydrogels. *Pharmaceutics* **2021**, *13*, 1602. [CrossRef]
17. Salave, S.; Rana, D.; Sharma, A.; Bharathi, K.; Gupta, R.; Khode, S.; Benival, D.; Kommineni, N. Polysaccharide Based Implantable Drug Delivery: Development Strategies, Regulatory Requirements, and Future Perspectives. *Polysaccharides* **2022**, *3*, 625–654. [CrossRef]
18. Fernandes, M.; Souto, A.P.; Dourado, F.; Gama, M. Application of Bacterial Cellulose in the Textile and Shoe Industry: Development of Biocomposites. *Polysaccharides* **2021**, *2*, 566–581. [CrossRef]
19. Marques, C.S.; Silva, R.R.A.; Arruda, T.R.; Ferreira, A.L.V.; Oliveira, T.V.; Moraes, A.R.F.; Dias, M.V.; Vanetti, M.C.D.; Soares, N.D.F.F. Development and Investigation of Zein and Cellulose Acetate Polymer Blends Incorporated with Garlic Essential Oil and β-Cyclodextrin for Potential Food Packaging Application. *Polysaccharides* **2022**, *3*, 277–291. [CrossRef]

20. Field, J.L.; Richard, T.L.; Smithwick, E.A.H.; Cai, H.; Laser, M.S.; LeBauer, D.S.; Long, S.P.; Paustian, K.; Qin, Z.; Sheehan, J.J.; et al. Robust Paths to Net Greenhouse Gas Mitigation and Negative Emissions Via Advanced Biofuels. *Proc. Natl. Acad. Sci. USA* **2020**, *117*, 21968–21977. [CrossRef]
21. Xu, C.; Strømme, M. Sustainable Porous Carbon Materials Derived from Wood-Based Biopolymers for CO_2 Capture. *Nanomaterials* **2019**, *9*, 103. [CrossRef] [PubMed]
22. Heo, Y.J.; Park, S.J. A Role of Steam Activation on CO_2 Capture and Separation of Narrow Microporous Carbons Produced from Cellulose Fibers. *Energy* **2015**, *91*, 142–150. [CrossRef]
23. Zhuo, H.; Hu, Y.; Tong, X.; Zhong, L.; Peng, X.; Sun, R. Sustainable Hierarchical Porous Carbon Aerogel from Cellulose for High-Performance Supercapacitor and CO_2 Capture. *Ind. Crops Prod.* **2016**, *87*, 229–235. [CrossRef]
24. Sevilla, M.; Fuertes, A.B. Sustainable Porous Carbons with A Superior Performance for CO_2 Capture. *Energy Environ. Sci.* **2011**, *4*, 1765–1771. [CrossRef]
25. Xu, C.; Ruan, C.Q.; Li, Y.; Lindh, J.; Strømme, M. High-Performance Activated Carbons Synthesized from Nanocellulose for CO_2 Capture and Extremely Selective Removal of Volatile Organic Compounds. *Adv. Sustain. Syst.* **2018**, *2*, 1700147. [CrossRef]
26. Ho, N.A.D.; Leo, C.P. A Review on the Emerging Applications of Cellulose, Cellulose Derivatives and Nanocellulose in Carbon Capture. *Environ. Res.* **2021**, *197*, 111100. [CrossRef]
27. Kamran, U.; Park, S.J. Acetic Acid-Mediated Cellulose-Based Carbons: Influence of Activation Conditions on Textural Features and Carbon Dioxide Uptakes. *J. Colloid Interface Sci.* **2021**, *594*, 745–758. [CrossRef]
28. Wang, C.; Okubayashi, S. Polyethyleneimine-Crosslinked Cellulose Aerogel for Combustion CO_2 Capture. *Carbohydr. Polym.* **2019**, *225*, 115248. [CrossRef]
29. Sun, Y.; Chu, Y.; Wu, W.; Xiao, H. Nanocellulose-Based Lightweight Porous Materials: A Review. *Carbohydr. Polym.* **2020**, *255*, 117489. [CrossRef]
30. Sepahvand, S.; Bahmani, M.; Ashori, A.; Pirayesh, H.; Yu, Q.; Dafchahi, M.N. Preparation and Characterization of Air Nanofilters Based on Cellulose Nanofibers. *Int. J. Biol. Macromol.* **2021**, *182*, 1392–1398. [CrossRef]
31. Chen, X.; Lin, J.; Wang, H.; Yang, Y.; Wang, C.; Sun, Q.; Shen, X.; Li, Y. Epoxy-Functionalized Polyethyleneimine Modified Epichlorohydrin-Cross-Linked Cellulose Aerogel as Adsorbents for Carbon Dioxide Capture. *Carbohydr. Polym.* **2023**, *302*, 120389. [CrossRef] [PubMed]
32. Ansaloni, L.; Gay, J.S.; Ligi, S.; Baschetti, M.G. Nanocellulose-Based Membranes for CO_2 Capture. *J. Membr. Sci.* **2017**, *522*, 216–225. [CrossRef]
33. Venturi, D.; Grupkovic, D.; Sisti, L.; Baschetti, M.G. Effect of Humidity and Nanocellulose Content on Polyvinylamine-Nanocellulose Hybrid Membranes for CO_2 Capture. *J. Membr. Sci.* **2018**, *548*, 263–274. [CrossRef]
34. Venturi, D.; Chrysanthou, A.; Dhuiège, B.; Missoum, K.; Baschetti, M.G. Arginine/Nanocellulose Membranes for Carbon Capture Applications. *Nanomaterials* **2019**, *9*, 877. [CrossRef] [PubMed]
35. Hussain, A.; Farrukh, S.; Hussain, A.; Ayoub, M. Carbon Capture from Natural Gas Using Multi-Walled CNTs Based Mixed Matrix Membranes. *Environ. Technol.* **2017**, *40*, 843–854. [CrossRef]
36. Mubashir, M.; Dumée, L.F.; Fong, Y.Y.; Jusoh, N.; Lukose, J.; Chai, W.S.; Show, P.L. Cellulose Acetate-Based Membranes by Interfacial Engineering and Integration Of ZIF-62 Glass Nanoparticles for CO_2 Separation. *J. Hazard Mater.* **2021**, *415*, 125639. [CrossRef]
37. Rehman, A.; Jahan, Z.; Sher, F.; Noor, T.; Niazi, M.B.K.; Akram, M.A.; Sher, E.K. Cellulose Acetate Based Sustainable Nanostructured Membranes for Environmental Remediation. *Chemosphere* **2022**, *307*, 135736. [CrossRef]
38. Wang, S.; Wang, C.; Zhou, Q. Strong Foam-Like Composites from Highly Mesoporous Wood and Metal-Organic Frameworks for Efficient CO_2 Capture. *ACS Appl. Mater. Interfaces* **2021**, *13*, 29949–29959. [CrossRef]
39. Li, A.; Lin, R.; Lin, C.; He, B.; Zheng, T.; Lu, L.; Cao, Y. An Environment-Friendly and Multi-Functional Absorbent from Chitosan for Organic Pollutants and Heavy Metal Ion. *Carbohydr. Polym.* **2016**, *148*, 272–280. [CrossRef]
40. Li, D.; Zhou, J.; Zhang, Z.; Li, L.; Tian, Y.; Lu, Y.; Qiao, Y.; Li, J.; Wen, L. Improving Low-Pressure CO_2 Capture Performance of N-Doped Active Carbons by Adjusting Flow Rate of Protective Gas During Alkali Activation. *Carbon* **2017**, *114*, 496–503. [CrossRef]
41. Wu, Q.; Zhang, G.; Gao, M.; Huang, L.; Li, L.; Liu, S.; Xie, C.; Zhang, Y.; Yu, S. N-Doped Porous Carbon from Different Nitrogen Sources for High-Performance Supercapacitors and CO_2 Adsorption. *J. Alloys Compd.* **2019**, *786*, 826–838. [CrossRef]
42. Lourenço, M.A.O.; Nunes, C.; Gomes, J.R.B.; Pires, J.; Pinto, M.L.; Ferreira, P. Pyrolyzed Chitosan-Based Materials for CO_2/CH_4 Separation. *Chem. Eng. J.* **2019**, *362*, 364–374. [CrossRef]
43. Wang, P.; Zhang, G.; Chen, W.; Chen, Q.; Jiao, H.; Liu, L.; Wang, X.; Deng, X. Molten Salt Template Synthesis of Hierarchical Porous Nitrogen-Containing Activated Carbon Derived from Chitosan for CO_2 Capture. *ACS Omega* **2020**, *5*, 23460–23467. [CrossRef] [PubMed]
44. Chagas, J.A.O.; Crispim, G.O.; Pinto, B.P.; Gil, R.A.S.S.; Mota, C.J.A. Synthesis, Characterization, and CO_2 Uptake of Adsorbents Prepared by Hydrothermal Carbonization of Chitosan. *ACS Omega* **2020**, *5*, 29520–29529. [CrossRef] [PubMed]
45. Kamran, U.; Park, S.J. Tuning Ratios of KOH and NaOH on Acetic Acid-Mediated Chitosan-Based Porous Carbons for Improving Their Textural Features and CO_2 Uptakes. *J. CO_2 Util.* **2020**, *40*, 101212. [CrossRef]
46. Islam, M.A.; Tan, Y.L.; Islam, M.A.; Romić, M.; Hameed, B.H. Chitosan–Bleaching Earth Clay Composite as An Efficient Adsorbent for Carbon Dioxide Adsorption: Process Optimization. *Colloids Surf. A Physicochem. Eng. Asp.* **2018**, *554*, 9–15. [CrossRef]

47. Zhao, B.; Borghei, M.; Zou, T.; Wang, L.; Johansson, L.S.; Majoinen, J.; Sipponen, M.H.; Österberg, M.; Mattos, B.D.; Rojas, O.J. Lignin-Based Porous Supraparticles for Carbon Capture. *ACS Nano* **2021**, *15*, 6774–6786. [CrossRef]
48. Shao, L.; Liu, N.; Wang, L.; Sang, Y.; Wan, H.; Zhan, P.; Zhang, L.; Huang, J.; Chen, J. Facile Preparation of Oxygen-Rich Porous Polymer Microspheres from Lignin-Derived Phenols for Selective CO_2 Adsorption and Iodine Vapor Capture. *Chemosphere* **2022**, *288*, 132499. [CrossRef]
49. Liu, N.; Shao, L.; Wang, C.; Sun, F.; Wu, Z.; Zhan, P.; Zhang, L.; Wan, H. Preparation of Lignin Modified Hyper-Cross-Linked Nanoporous Resins and Their Efficient Adsorption for P-Nitrophenol in Aqueous Solution and CO_2 Capture. *Int. J. Biol. Macromol.* **2022**, *221*, 25–37. [CrossRef]
50. Poulson, B.G.; Alsulami, Q.A.; Sharfalddin, A.; El Agammy, E.F.; Mouffouk, F.; Emwas, A.-H.; Jaremko, L.; Jaremko, M. Cyclodextrins: Structural, Chemical, and Physical Properties, and Applications. *Polysaccharides* **2022**, *3*, 1–31. [CrossRef]
51. Liu, C.; Cao, S.; Zhou, L.; Zhang, H.; Zhao, Y.; Han, J. Cyclodextrin-Based Aerogels: A Review of Nanomaterials Systems and Applications. *ACS Appl. Nano Mater.* **2022**, *5*, 13921–13939. [CrossRef]
52. Li, L.; Wang, J.; Zhang, Z.; Yang, Q.; Yang, Y.; Su, B.; Bao, Z.; Ren, Q. Inverse Adsorption Separation of CO_2/C_2H_2 Mixture in Cyclodextrin-Based Metal-Organic Frameworks. *ACS Appl. Mater. Interfaces* **2018**, *11*, 2543–2550. [CrossRef] [PubMed]
53. Guo, T.; Bedane, A.H.; Pan, Y.; Shirani, B.; Xiao, H.; Eić, M. Adsorption Characteristics of Carbon Dioxide Gas on a Solid Acid Derivative of β-Cyclodextrin. *Energy Fuels* **2017**, *31*, 4186–4192. [CrossRef]
54. Hamedi, A.; Anceschi, A.; Trotta, F.; Hasanzadeh, M.; Caldera, F. Rapid Temperature-Assisted Synthesis of Nanoporous γ-Cyclodextrin-Based Metal–Organic Framework for Selective CO_2 Adsorption. *J. Incl. Phenom. Macrocycl. Chem.* **2021**, *99*, 245–253. [CrossRef]
55. Du, Y.; Geng, Y.; Guo, T.; Zhang, R.; Zhang, Y.; Wang, X.; Han, Z. Thermodynamic Characteristics of CO_2 Adsorption on B-Cyclodextrin Based Porous Materials: Equilibrium Capacity Function with Four Variables. *Case Stud. Therm. Eng.* **2022**, *39*, 102426. [CrossRef]
56. Guo, T.; Zhang, R.; Wang, X.; Kong, L.; Xu, J.; Xiao, H.; Bedane, A.H. Porous Structure of β-Cyclodextrin for CO_2 Capture: Structural Remodeling by Thermal Activation. *Molecules* **2022**, *27*, 7375. [CrossRef]
57. Gao, H.; Li, Q.; Ren, S. Progress on CO_2 Capture by Porous Organic Polymers. *Curr. Opin. Green Sustain. Chem.* **2019**, *16*, 33–38. [CrossRef]
58. Hu, Z.; Wang, Y.; Wang, X.; Zhai, L.; Zhao, D. Solution-Reprocessable Microporous Polymeric Adsorbents for Carbon Dioxide Capture. *AIChE J.* **2018**, *64*, 3376–3389. [CrossRef]
59. Fayemiwo, K.A.; Vladisavljević, G.T.; Nabavi, S.A.; Benyahia, B.; Hanak, D.P.; Loponov, K.N.; Manović, V. Nitrogen-Rich Hyper-Crosslinked Polymers for Low-Pressure CO_2 Capture. *Chem. Eng. J.* **2018**, *334*, 2004–2013. [CrossRef]
60. Liu, Y.; Chen, X.; Jia, X.; Fan, X.; Zhang, B.; Zhang, A.; Zhang, Q. Hydroxyl-Based Hypercrosslinked Microporous Polymers and Their Excellent Performance for CO_2 Capture. *Ind. Eng. Chem. Res.* **2018**, *57*, 17259–17265. [CrossRef]
61. Abdelnaby, M.M.; Alloush, A.M.; Qasem, N.A.A.; Al-Maythalony, B.A.; Mansour, R.B.; Cordova, K.E.; Al Hamouz, O.C.S. Carbon dioxide Capture in The Presence of Water by An Amine-Based Crosslinked Porous Polymer. *J. Mater. Chem. A* **2018**, *6*, 6455–6462. [CrossRef]
62. Abdelnaby, M.M.; Qasem, N.A.A.; Al-Maythalony, B.A.; Cordova, K.E.; Al Hamouz, O.C.S. A Microporous Organic Copolymer for Selective CO_2 Capture Under Humid Conditions. *ACS Sus. Chem. Eng.* **2019**, *7*, 13941–13948. [CrossRef]
63. Kong, X.; Li, S.; Strømme, M.; Xu, C. Synthesis of Porous Organic Polymers with Tunable Amine Loadings for CO_2 Capture: Balanced Physisorption and Chemisorption. *Nanomaterials* **2019**, *9*, 1020. [CrossRef] [PubMed]
64. Sang, Y.; Shao, L.; Huang, J. Carbonyl Functionalized Hyper-Cross-Linked Polymers for CO_2 Capture. *J. Polym. Res.* **2020**, *27*, 188. [CrossRef]
65. Sharma, N.; Ugale, B.; Kumar, S.; Kailasam, K. Metal-Free Heptazine-Based Porous Polymeric Network as Highly Efficient Catalyst for CO_2 Capture and Conversion. *Front. Chem.* **2021**, *9*, 737511. [CrossRef]
66. Shao, L.; Sang, Y.; Liu, N.; Wei, Q.; Wang, F.; Zhan, P.; Luo, W.; Huang, J.; Chen, J. One-step synthesis of N-containing Hyper-Cross-Linked Polymers by Two Crosslinking Strategies and Their CO_2 Adsorption and Iodine Vapor Capture. *Sep. Purif. Technol.* **2021**, *262*, 118352. [CrossRef]
67. Mohamed, M.G.; Ahmed, M.M.M.; Du, W.-T.; Kuo, S.-W. Meso/Microporous Carbons from Conjugated Hyper-Crosslinked Polymers Based on Tetraphenylethene for High-Performance CO_2 Capture and Supercapacitor. *Molecules* **2021**, *26*, 738. [CrossRef]
68. Qiao, Y.; Zhan, Z.; Yang, Y.; Liu, M.; Huang, Q.; Ke, B.T.X.; Wu, C. Amine or Azo Functionalized Hypercrosslinked Polymers for Highly Efficient CO_2 Capture and Selective CO_2 Capture. *Mater. Today* **2021**, *27*, 102338. [CrossRef]
69. Zhou, H.; Rayer, C.; Antonangelo, A.R.; Hawkins, N.; Carta, M. Adjustable Functionalization of Hyper-Cross-Linked Polymers of Intrinsic Microporosity for Enhanced CO_2 Adsorption and Selectivity Over N_2 and CH_4. *ACS Appl. Mater. Interfaces* **2022**, *14*, 20997–21006. [CrossRef]
70. Abdelnaby, M.M.; Saleh, T.A.; Zeama, M.; Abdalla, M.A.; Ahmed, H.M.; Habib, M.A. Azo-Linked Porous Organic Polymers for Selective Carbon Dioxide Capture and Metal Ion Removal. *ACS Omega* **2022**, *7*, 14535–14543. [CrossRef]
71. Gao, Q.; Li, X.; Ning, G.-H.; Xu, H.-S.; Liu, C.; Tian, B.; Tang, W.; Loh, K.P. Covalent Organic Framework with Frustrated Bonding Network for Enhanced Carbon Dioxide Storage. *Chem. Mater.* **2018**, *30*, 1762–1768. [CrossRef]
72. Li, Y.; Zhang, J.; Zuo, K.; Li, Z.; Wang, Y.; Hu, H.; Zeng, C.; Xu, H.; Wang, B.; Gao, Y. Covalent Organic Frameworks for Simultaneous CO_2 Capture and Selective Catalytic Transformation. *Catalysts* **2021**, *11*, 1133. [CrossRef]

73. Lyu, H.; Li, H.; Hanikel, N.; Wang, K.; Yaghi, O.M. Covalent Organic Frameworks for Carbon Dioxide Capture from Air. *J. Am. Chem. Soc.* **2022**, *144*, 12989–12995. [CrossRef]
74. Xu, Y.; Li, Z.; Zhang, F.; Zhuang, X.; Zeng, Z.; Wei, J. New Nitrogen-Rich Azo-Bridged Porphyrin-Conjugated Microporous Networks for High Performance of Gas Capture and Storage. *RSC Adv.* **2016**, *6*, 30048–30055. [CrossRef]
75. Wang, S.; Liu, Y.; Yu, Y.; Du, J.; Cui, Y.; Songa, X.; Liang, Z. Conjugated Microporous Polymers Based on Biphenylene for CO_2 Adsorption and Luminescent Detection of Nitroaromatic Compounds. *New J. Chem.* **2018**, *42*, 9482–9487. [CrossRef]
76. Ren, S.-B.; Li, P.-X.; Stephenson, A.; Chen, L.; Briggs, M.E.; Clowes, R.; Alahmed, A.; Li, K.-K.; Jia, W.-P.; Han, D.-M. A 1,3-Diyne-Linked Conjugated Microporous Polymer for Selective CO_2 Capture. *Ind. Eng. Chem. Res.* **2018**, *57*, 9254–9260. [CrossRef]
77. Saber, A.F.; Chen, K.-Y.; EL-Mahdy, A.F.M.; Kuo, S.-W. Designed Azo-Linked Conjugated Microporous Polymers for CO_2 Uptake and Removal Applications. *J. Polym. Res.* **2021**, *28*, 430. [CrossRef]
78. Das, S.K.; Bhanja, P.; Kundu, S.K.; Mondal, S.; Bhaumik, A. Role of Surface Phenolic-OH Groups in N-Rich Porous Organic Polymers for Enhancing the CO_2 Uptake and CO_2/N_2 Selectivity: Experimental and Computational Studies. *ACS Appl. Mater. Interfaces* **2018**, *10*, 23813–23824. [CrossRef] [PubMed]
79. Yao, C.; Li, G.; Wang, J.; Xu, Y.; Chang, L. Template-Free Synthesis of Porous Carbon from Triazine Based Polymers and Their Use in Iodine Adsorption and CO_2 Capture. *Sci. Rep.* **2018**, *8*, 1867. [CrossRef]
80. Tuci, G.; Iemhoff, A.; Ba, H.; Luconi, L.; Rossin, A.; Papaefthimiou, V.; Palkovits, R.; Artz, J.; Pham-Huu, C.; Giambastiani, G. Playing with Covalent Triazine Framework Tiles for Improved CO_2 Adsorption Properties and Catalytic Performance. *Beilstein J. Nanotechnol.* **2019**, *10*, 1217–1227. [CrossRef]
81. Dang, Q.-Q.; Liu, C.-Y.; Wang, X.-M.; Zhang, X.-M. Novel Covalent Triazine Framework for High Performance CO_2 Capture and Alkyne Carboxylation Reaction. *ACS Appl. Mater. Interfaces* **2018**, *10*, 27972–27978. [CrossRef] [PubMed]
82. Xu, G.; Zhu, Y.; Xie, W.; Zhang, S.; Yao, C.; Xu, Y. Porous Cationic Covalent Triazine-Based Frameworks as Platforms for Efficient CO_2 And Iodine Capture. *Chem. Asian J.* **2019**, *14*, 3259–3263. [CrossRef] [PubMed]
83. Zhu, H.; Lin, W.; Li, Q.; Hu, Y.; Guo, S.; Wang, C.; Yan, F. Bipyridinium-Based Ionic Covalent Triazine Frameworks for CO_2, SO_2 and NO Capture. *ACS Appl. Mater. Interfaces* **2020**, *12*, 8614–8621. [CrossRef] [PubMed]
84. Liao, C.; Liang, Z.; Liu, B.; Chen, H.; Wang, X.; Li, H. Phenylamino-, Phenoxy-, and Benzenesulfenyl-Linked Covalent Triazine Frameworks for CO_2 Capture. *ACS Appl. Nano Mater.* **2020**, *3*, 2889–2898. [CrossRef]
85. Wessely, I.D.; Schade, A.M.; Dey, S.; Bhunia, A.; Nuhnen, A.; Janiak, C.; Bräse, S. Covalent Triazine Frameworks Based on The First Pseudo-Octahedral Hexanitrile Monomer via Nitrile Trimerization: Synthesis, Porosity, and CO_2 Gas Sorption Properties. *Materials* **2021**, *14*, 3214. [CrossRef]
86. Mohamed, M.G.; Sharma, S.U.; Liu, N.-Y.; Mansoure, T.H.; Samy, M.M.; Chaganti, S.V.; Chang, Y.-L.; Lee, J.-T.; Kuo, S.-W. Ultrastable Covalent Triazine Organic Framework Based on Anthracene Moiety as Platform for High-Performance Carbon Dioxide Adsorption and Supercapacitors. *Int. J. Mol. Sci.* **2022**, *23*, 3174. [CrossRef]

Disclaimer/Publisher's Note: The statements, opinions and data contained in all publications are solely those of the individual author(s) and contributor(s) and not of MDPI and/or the editor(s). MDPI and/or the editor(s) disclaim responsibility for any injury to people or property resulting from any ideas, methods, instructions or products referred to in the content.